Crystal structure of a novel cysteinless plant Kunitz-type protease inhibitor

Daiane Hansen [a], Sandra Macedo-Ribeiro [b,c], Paula Veríssimo [b], Sonia Yoo Im [a], Misako Uemura Sampaio [a], Maria Luiza Vilela Oliva [a,*]

[a] *Departamento de Bioquímica, Universidade Federal de São Paulo-Escola Paulista de Medicina, Rua Três de Maio, 100, 04044-020 São Paulo, SP, Brazil*
[b] *Departamento de Bioquímica e Centro de Neurociências e Biologia Celular, Universidade de Coimbra, 3004-517 Coimbra, Portugal*
[c] *Instituto de Biologia Molecular e Celular—IBMC, Rua do Campo Alegre 823, 4150-180 Porto, Portugal*

Abstract

Bauhinia bauhinioides Cruzipain Inhibitor (BbCI) is a cysteine protease inhibitor highly homologous to plant Kunitz-type inhibitors. However, in contrast to classical Kunitz family inhibitors it lacks cysteine residues and therefore disulfide bridges. BbCI is also distinct in the ability to inactivate enzymes belonging to two different classes, cysteine and serine proteases. Besides inhibiting the cysteine protease cruzipain, BbCI also inhibits cathepsin L and the serine proteases HNE (human neutrophil elastase) and PPE (porcine pancreatic elastase). Monoclinic crystals of the recombinant inhibitor that diffract to 1.7 Å resolution were obtained using hanging drop method by vapor diffusion at 18 °C. The refined structure shows the conservative β-trefoil fold features of the Kunitz inhibitors. In BbCI, one of the two characteristic S–S bonds is replaced by the water-mediated interaction between Tyr125 and Gly132. In this work we explore the structural differences between Kunitz-type inhibitors and analyze the essential interactions that maintain the protein structural stability preserving its biological function.
© 2007 Elsevier Inc. All rights reserved.

Keywords: Cathepsin; Crystallography; Cruzipain; Elastase; Kallikrein; Kunitz protease inhibitors; X-ray diffraction

Protease inhibitors have been isolated from diverse sources and they have been associated with diverse events as plant evolution [1,2] and protection against microorganism invasion and insect attack [3,4]. Among the many classes of plant inhibitors, the Kunitz family is the best characterized probably due their abundance in seeds [1,2].

Extracts from some *Bauhinia* species are used in traditional medicine for the diabetes treatment [5,6]. We previously isolated an inhibitor from seeds of *Bauhinia bauhinioides*, Cesalpinoideae, a plant known in Brazil by the trivial name of ''cow paw'' due the shape of its leaves [7]. This inhibitor was named BbCI, *Bauhinia bauhinioides* Cruzipain Inhibitor [8], since it inhibits cruzipain, the major cysteine protease isolated of *Trypanosoma cruzi*

and cruzain (Ki_{app} 0.3 nM), its recombinant form [9]. *Trypanosoma cruzi* is the causative agent of Chagas' disease, the parasitic infection that remains as one of the leading causes of heart disease in Latin America [10].

Most curiously, this BbCI shows inhibitory properties against enzymes of two different classes, cysteine and serine proteases. We have verified that BbCI inhibits porcine pancreatic elastase (Ki_{app} 40 nM), and human neutrophil elastase (Ki_{app} 5.3 nM), a key enzyme involved in inflammatory processes [8,11]. In vitro, BbCI also inhibits cathepsin L (Ki_{app} 2.2 nM) [8], and in contrast, it does not affect the activity of cathepsin B, cathepsin V and cathepsin X, very similar papain-like proteases [8].

We previously reported a *Bauhinia bauhinioides* Kallikrein Inhibitor, BbKI, an 18 kDa protein isolated from the same plant seeds, that although displaying a high (84%) primary structure identity, differs from BbCI by inhibiting plasma kallikrein (Ki_{app} 2.4 nM) and plasmin

* Corresponding author. Fax: +55 11 5572 3006.
  E-mail address: olivaml.bioq@epm.br (M.L.V Oliva).

(Ki$_{app}$ 33 nM) [12,13]. Those inhibitory properties demonstrated by these atypical Kunitz inhibitors were confirmed by the recombinant proteins [14].

One of the distinct features of the plant Kunitz (STI) family is the presence of two highly conserved disulfide bridges. We have characterized a new subclass of Kunitz inhibitor with only one disulfide bridge [15,16] or no disulfide bridges [17]. The BbCI primary structure presents no cysteine residues, and BbKI bears only one cysteine residue in the C-terminal region. The absence of cysteine residues distinguishes BbCI from classical Kunitz inhibitors where the disulfide bridges contribute to their stability and biological activity.

Here, we report the three-dimensional structure of the recombinant BbCI to 1.70 Å resolution and compare it to the structure of the highly homologous BbKI. The three-dimensional structures of only a few plant Kunitz-type inhibitors have been determined and they all display a β-trefoil structure [18–20], composed of a six-stranded β-barrel closed at one end by three β-hairpins and exhibiting a characteristic pseudo 3-fold axis of symmetry when viewed down the β-barrel axis [21]. All representative proteins of the β-trefoil family display the same 3-fold repetition as a distinctive structural signature although they are less than 30% identical at the amino acid sequence level [22].

To the best of our knowledge, this is the first report of a crystallographic structure of an inhibitor of the Kunitz (STI) family without disulfide bridges. Given the importance of the covalent bonds in the stabilization of the reactive site loop [23,24], it was important to elucidate the rBbCI crystallographic structure in order to understand the structural aspects surrounding its reactive site.

Results and discussion

rBbCI structure displays a beta-trefoil fold

rBbCI structure contains 164 residues, numbered from Met (0) to Thr (163). All residues were unambiguously resolved by electron density maps. As in contrast to classical Kunitz-type inhibitors, BbCI has no cysteine residues and therefore no disulfide bridges, in order to further understand the detailed structural features of this cysteinless inhibitor we have solved the crystal structure of rBbCI at 1.7 Å resolution (Fig. 1). The crystallographic structure was refined to an *R*-value of 20.7% (*R*$_{free}$ 25.6%) using all reflections between 26.8 and 1.7 Å (for a detailed view of data collection and refinement statistics please refer to Table 1). A detailed view of the final electron density map is shown in Fig. 2A highlighting the overall quality of the experimental data. The asymmetric unit contains two molecules of rBbCI and 239 solvent molecules. The rBbCI structure presents a typical "β-trefoil" fold, as shown in Fig. 1. It is formed by six two-stranded hairpins, three of these form a barrel structure, and the other three are in a triangular array that caps the barrel. The
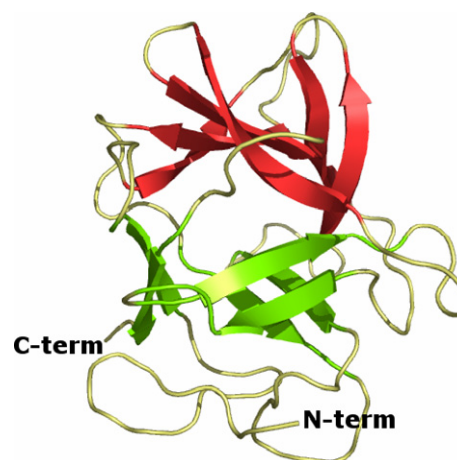

Fig. 1. The overall structure of rBbCI. rBbCI has a β-trefoil fold, formed by six two-stranded hairpins. Three of these form a barrel structure (in green) and the other three are in a triangular array that caps the barrel (in red). (For interpretation of the references in color in this figure legend, the reader is referred to the web version of this article.)

Table 1
Data collection and refinement statistics

Data collection	Monoclinic
Group space	P2$_1$
Resolution (Å)	26.82–1.7 (2.06 − 1.7)[a]
Unit-cell parameters (Å, °)	$a = 61.96$, $b = 41.32$, $c = 63.53$, $\beta = 98.46$
R_{sym}[b] (%)	8.2 (43.4)[a]
Number of observations	505658
Unique reflections	37751
Completeness (%)	95.2 (91.9)[a]
*R*merge (%)	8.2 (43.4)
I/σ (I)	7.0 (1.7)
Refinement	
Final R[c], R_{free} ($F > 0$)	0.207, 0.256
Number of of residues per monomer	163
Number of solvent molecules	239
Average *B* values (Å2): Protein	19.11
Average *B* values (Å2): Water	29.56
R.m.s.d. bonds (Å)	0.022
R.m.s.d. angles (°)	1.98
Ramachandran plot (%)	
Residues in most favorable regions	92.2
Residues in additional allowed regions	7.4
Residues in generously allowed regions	0.4
Residues in disallowed regions	0

[a] Numbers in parentheses refer to the highest resolution shell.
[b] Rsym $= \sum |I - (I)| / \sum|$. (*I*) is the average intensity of symmetry-related observations of a unique reflection.
[c] $R = \sum |F_o - F_c| / \sum F_o$. R_{free} is calculated as R but for 10% of the reflections excluded from all refinement.

arrangement of the secondary structure gives the molecule a pseudo 3-fold axis. The amino acid Asp16, in both molecules in the asymmetric unit, is present in generously allowed region of the Ramachandran map [25], although it is perfectly well defined in the electron density map. This can be explained by the presence of a strong crystalline contact with the region of the loop formed with the amino
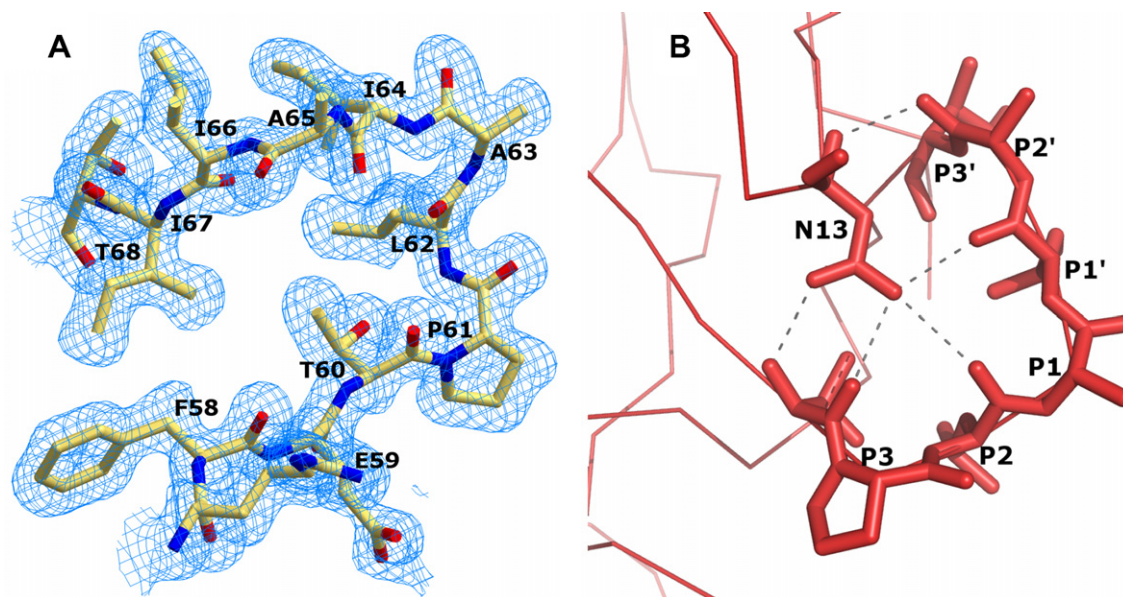
Fig. 2. (A) Electron density map, contoured at 1σ, of the rBbCI reactive site loop showing alanine 63 at position P1. (B) Residue Asn13 forms a network of hydrogen bonds (dashed lines) scaffolding along with the reactive site loop (P3–P3́) of rBbCI.

acids Ser81, Ser82 and Asp83 of the symmetrically equivalent molecule.

Structural comparison of rBbCI with other plant Kunitz-type inhibitors

Despite their low sequence homology, crystallographic analyses of the Kunitz inhibitors from soybean [24], and *Erythrina caffra* [23], the interleukins-1β and 1α [26] and the acid and basic fibroblast growth factors [27] have shown that they share this unusual fold. BbCI shares a high structural homology with the plant Kunitz-type inhibitors BbKI, SbTI and ETI. The inhibitors rBbCI and rBbKI are 18 kDa proteins with high structural identity and contain conserved residues characteristics of the plant Kunitz-type inhibitor family, for example Asp5, Gly8, Pro10, Tyr17, Tyr18, Gly28 and Gly35/Asn36/Glu37 (SbTI numbering), but they do not contain any disulfide bridges. The residues Cys40, Cys80, Cys125 and Cys132 are substituted by Glu40, Ser80, Tyr125 and Gly132 in both rBbCI and rBbKI structures, as shown in Fig. 3. The superposition of the structurally equivalent Cα atoms of rBbCI with rBbKI and ETI gives an r.m.s. deviation of 0.88 and 1.9 Å, respectively. The central scaffold is common and larger deviations occur within the surface loops where overall sequence conservation is lower.

The major differences in rBbCI and rBbKI three-dimensional structures is the loop which, in the case of rBbCI, is formed by the amino acids Val78, Pro79, Ser80, Ser81, Ser82, Asp83, Ser84, Glu85 and in rBbKI by Gly78, Pro79, Ser80, Ser81, Ser82, Asp83, Ser84, Gly85 (Fig. 3). The change of Val78 and Glu85 in rBbCI to glycine in rBbKI permits different orientations in this loop-80. rBbKI loop is more flexible while in rBbCI the

loop shows less mobility and is closer to the main core of the protein.

Structural consequences of disulfide bond replacement

In the classical Kunitz inhibitors such STI and ETI, the two disulfide bridges are localized on the surface of the protein, what makes them highly solvent-accessible, but the contribution of these structures on the maintenance of their functionality are on dependence of individual features of each protein. Thus, analysis of structural differences at this position may contribute to understand the significance of the disulfide bonds for the stability and inhibitory specificity of the proteins. Studies which had examined the role of disulfide bonds in the structure and unfolding of STI showed that the reduction of the disulfide bonds results in a fully inactive protein [28]. This result is in contrast to that shown in ETI, which remains fully active in both the disulfide intact and reduced states [29]. Thus, the disulfide bonds in STI play a crucial role in protein structure stabilization necessary to maintain enzymatic activity [28].

The absence of disulfide bridges in rBbCI and rBbKI might result in unfolded proteins and consequent loss of β-sheet structure. However, the replacement of Cys39, Cys83, Cys132 and Cys139 (ETI numbering, IDE3_ERYCA in Fig. 3) by Glu40, Ser80, Tyr125 and Gly132 in rBbCI and rBbKI, and which allowed the formation of hydrogen bonds, prevented a hydrophobic collapse of the protein, as it occurs with STI after the disulfide bonds were reduced. Tyr125 residue appears to be important for stabilization of rBbCI and rBbKI since the loop conformation is constrained by a water-mediated hydrogen bond between the Tyr125 and Gly132

```
                                                      40
IDE3_ERYCA  -VLLDGNGEVV-QNGGTYYLLPQVWAQGGGVQLAKTGEETCPLTVVQSPNELSDGKPIRI  58
IDE3_ERYLA  -VLLDGNGEVV-QNGGTYYLLPQVWAQGGGVQLAKTGEETCPLTVVQSPNELSDGKPIRI  58
IDE3_ERYVA  -VLLDGNGEVV-QNGGTYYLLPQVWAQGGGVQLAKTGEETCPLTVVQSPNELSNGKPIRI  58
IT1B_ERYVA  -ELVDVEGEDV-VNGGTYYMLPGIEGDGGGMEGAKTGRETCPITVVQSRNDVSNGEPITI  58
ITRY_BAUVA  DTLLDTDGEVVRNNGGPYYIIPAFRGNGGGLTLTRVGSETCPRTVVQASSEHSDGLPVVI  60
IFXA_BAUUN  DIVLDTDGKPV-NNGGQYYIIPAFRGNGGGLELTRVGRETCPHTVVQASSEISNGLPVMI  59
rBbKI       SVVVDTNGQPVSNGADAYYLVPVSHGHAG-LALAKIGNEAEPRAVVLDPHHRP-GLPVRF  58
rBbCI       SVILDTKGEPVSNAADAYYLVPVSHGEGG-LALAKVGNEAEPKAVVLDPHHRP-GLTVRF  58

            63          80
IDE3_ERYCA  ESRLRSAFIPDDDKVRIGFAYAPKCAPSP-WWTVVEDEQEGLSVKLSEDESTQFDYPFKF  117
IDE3_ERYLA  ESRLRSTFIPDDDEVRIGFAYAPKCAPSP-WWTVVEDEQEGLSVKLSEDESTQFDYPFKF  117
IDE3_ERYVA  ESRLRSAFIPDDDKVRIGFAYAPKCAPSP-WWTVVLEDEQEGLSVKLSEDESTQFDYPFKF  117
IT1B_ERYVA  ESPFRSYFIPKGSLVRIGFTSPPKCAPSP-WWTLALDRPQGLSVKLGEYESTEFNYSFKF  117
ITRY_BAUVA  SALPRSLFISTSWRVTIQFVEA-TCIPKPSFWHIPQDSELEGAVKVGAS-DERFPLEFRI  118
IFXA_BAUUN  AALFRTMFISTAWRVSIQFLKVPTCTPKPSYWHIPQDSDMEGSVEVRV--DERFPLEFRI  117
rBbKI       ESPLRINIIKESYFLNIKFG---PSSSDSGVWDVIQQDPIGLAVKVTD--TKSLLGPFKV  113
rBbCI       ETPLAIAIITESFFLNIKFV---PSSSDSEVWDVSKQYPIGLAVKVTD--TKSFVGPFRV  113

                      125         132
IDE3_ERYCA  EQVSDQLHSYKLLYCEG----KHEKCASIGINRDQKGYRRLVVTEDYPLTVVLKKDESS-  172
IDE3_ERYLA  EQVSDKLHSYKLLYCEG----KHEKCASIGINRDQKGYRRLVVTEDNPLTVVLKKDESS-  172
IDE3_ERYVA  EQVSDKLHSYKLLYCEG----KHEKCASIGINRDQKGYRRLVVTEDNPLTVVLKKDESS-  172
IT1B_ERYVA  EDVSSKLHSYKLSYCVREEWYEDYICKNIGIYRDSKGYRRLVVNEENPLVVVLKKVESS-  176
ITRY_BAUVA  ERVSED--TYKLMHCSS----TSDSCRDLGISIDEEGNRRLVVRDENPLLVRFKKANQDS  172
IFXA_BAUUN  EKVSED--AYKLMHCPS----SSDSCRDLGIAIDEENNRRLVVRDGKPLLVRFKEANQDS  171
rBbKI       EKEGEG---YKIVYYPE----RGQTGLDIGLVHRNDKYY-LAVKDGEPCVFKIRKATDE-  164
rBbCI       EKEGEG---YKIVYYPD----RGQTGLDIGLVHRNDKYY-LAATEGEPFVFKIRKATYE-  164
```

Fig. 3. The amino acid sequence alignment of rBbCI and rBbKI inhibitors with representative members of the plant-type Kunitz inhibitor family. The alignment was performed using ClustalW [43] (http://www.ebi.ac.uk/clustalw). Conserved amino acids are boxed in white the cysteine residues are within a black box and the amino acid in P1 is highlighted by a circle.
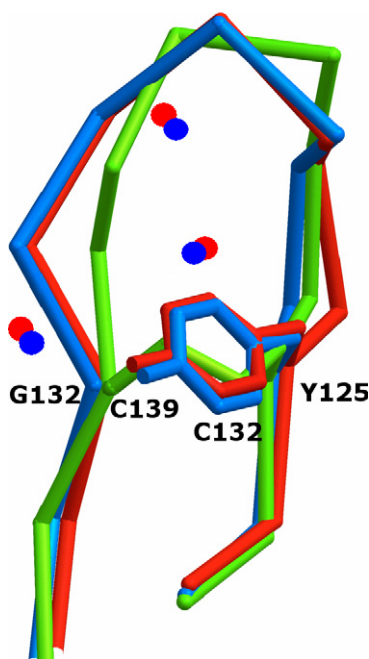

Fig. 4. A water-mediated hydrogen bond in *Bauhinia* inhibitors replace the disulfide bridges formed between Cys132 and Cys139 in ETI (green) rBbCI is shown in red and rBbKI in blue. The figures were prepared with the program Pymol [44]. (For interpretation of the references in color in this figure legend, the reader is referred to the web version of this article.)

(Fig. 4). This interaction replaces the ETI disulfide bridges involving residues Cys132 and Cys139 (ETI numbering). In the case of rBbCI and rBbKI, our studies clearly demonstrate that polar interaction of the protein is involved in the maintenance of the structural folding and therefore in the inhibitory function.

The other disulfide bridge, Cys39–Cys83 (ETI numbering), also common in classical plant-type Kunitz inhibitors, apparently reduces the flexibility of the loops by cross-linking the loops (loop-40 and loop-80) containing these residues. In both rBbCI and rBbKI, as a result of the missing disulfide bond, loop-80 moves away from loop-40, approaching the reactive site loop-60. Loop-80 is, the most divergent loop when compared to the structure of ETI.

Within BbKI loop-80, hydrogen bonds between Ser80 and Gly14 help to stabilize both loops, maintaining Asn13 in position to form a hydrogen bond network in the reactive site loop. In rBbCI, Ser80 forms a hydrogen bond with Ser82, within the same loop. The presence of the Gly14 in rBbKI and not in rBbCI confers higher flexibility to this loop, flexibility that is compensated in rBbKI by formation of a strong H-bond with Ser80.

In rBbCI, both loops 80 and 14 contain less glycine residues, therefore they are more rigid, loop-80 is internally stabilized by contacts with Ser82 and loop-14 is stabilized by a H-bond with the CO of Phe58 [14].

Comparison of the rBbCI, rBbKI and ETI reactive site

The geometry of the carbonyl group at the P1 position is relevant to generate an interaction between inhibitor and protease during catalysis [30,31]. The residues adjacent to P1 contribute to the inhibitory selectivity of the enzyme due to the characteristics of each amino acid establishing others interactions, such as hydrogen and saline bridges or steric influences that are fundamental to the inhibitory interaction. Alanine 63, identified as the P1 residue in the putative reactive site of rBbCI was confirmed by HNE and cruzipain/cruzain specific cleavage [11,14], as shown in Fig. 2A and B.

The maintenance of the canonical conformation of the reactive site loop is also considerable for the proper inhibitory function and protein scaffold plays a role at this position. Owing to its crucial position, the role of a conserved Asn (Asn13 in rBbCI and rBbKI and Asn12 in ETI) was emphasized in the Kunitz family of inhibitors [23,24,31]. In rBbCI crystallographic structure also keeps the stability, in addition with other interactions, of the loop formed between Thr60, Pro61, Leu62, Ala63, Ile64 and Ala65 of the reactive site, forming a hydrogen bond network, as shows Fig. 4.

Studies have pointed out the positive contribution of the hydrophobic characteristic of alanine at the P1 position for the interaction to the subsite S1 of elastase [32,33] and of cruzain [34]. Thus, the residue at P1 position of rBbCI reactive-site (Ala63) was mutated to examine its role in the inhibitory specificity. It was shown that this residue is crucial for elastase and cruzain inhibitory activity since rBbCI-A63R did not affect the enzyme substrate binding. However, the mutant inhibitor acquired the property for trypsin inhibition measured by the association constant, which is in the same order of magnitude than that of rBbKI (Ki_{app} 28 nM) [14], thereby supporting their reactive-site integrity and its role in the strict selectivity of BbCI, which is able to inhibit the serine proteases elastase and cathepsin G but not trypsin and trypsin like proteases.

Materials and methods

Crystallization. The rBbCI was obtained as described previously [14]. Crystals were grown by vapor diffusion at 18 °C temperature using the hanging drop method, in two different crystallization buffers: 0.1 M sodium acetate, pH 8.6 containing 0.2 M ammonium acetate and polyethylene glycol 4000 (30%), (rBbCI monoclinic) and 0.1 M Hepes, pH 7.5 containing 1.5 M lithium sulphate (rBbCI triclinic). Diffraction data were collected using a RIGAKU ultra X 18 rotating anode with a MAR345 dtb image plate. The resulting crystal (rBbCI monoclinic) belonged to space group $p2_1$ with cell dimensions of $a = 61.96$ Å, $b = 41.32$ Å, $c = 63.53$ Å, $\beta = 98.46°$ and with two inhibitor molecules, related by a non-crystallographic 2-fold symmetry axis, in unit asymmetric, which was the main object of this work (data shown in Table 1).

rBbCI triclinic crystals (space group $p321$) diffracted to lower resolution and data were not further used.

Data collection, processing, phasing, and refinement. rBbCI monoclinic data were collected at *IFSC Crystallography Laboratory* to 1.70 Å resolution and processed using the programs MOSFLM [35] and SCALA [36,37] from the CCP4 package [38].

The structure was solved by molecular replacement using the program MOLREP [39] and the crystal structure of rBbKI (recombinant *Bauhinia bauhinioides* Kallikrein Inhibitor) as a search model (PDB ID code 2GO2), both structures were solved at the same time, but rBbKI structure was determined by SIRAS [15]. Alternate rounds of model building with the program O [40] and further refinement with the program Refmac 5.0 [41] resulted in the final model with an R_{free} an R_{factor} of 25.6 and 20.7% for all data between 26.8 and 1.70 Å resolutions, respectively. The model was analyzed with Procheck [42] and showed 92.2% of the residues in core region of the Ramachandran plot [25], while the remaining 7.4% were present in the additionally allowed region. A single residue (Asp16) lies in the generously allowed region in both molecules A and B, but it is perfectly well defined in the electron density map. Coordinates have been deposited in the RCSB Protein Data Bank: PDB ID code 2GZB.

BbCI mutagenesis. The reactive site P1 residue encoding Ala63 was mutated to encode Arg63 through site-directed mutagenesis using a QuikChange Site-Directed Mutagenesis Kit (Stratagene, Germany) (BbCI-A63R) where the pET28aBbCI DNA double-stranded and 100 pmol of each primer containing the mutation desired (BbCI-A63R_FOWARD: 5′-CGG TTA GAT TTG AAA CCC CAC TTC GCA TTG CTA TAA TCA CAG AGT C-3′ BbCI-A63R_REVERSE: 5′-GAC TCT GTG ATT ATA GCA ATG CGA AGT GGG TTT TCA AAT CTA ACC G-3′) were used. The mutant protein rBbCI-A63R was expressed in *Escherichia coli* BL21 (DE3) and its specificity was assayed on cruzain, PPE and trypsin activity as described previously for rBbCI [8,11,12,14].

References

[1] M. Richardson, Seed storage proteins: the enzyme inhibitors. Methods in plant, Biochemistry 5 (1991) 259–305.

[2] Y. BirkIn Plant Protease Inhibitors: Significance in Nutrition, Plant Protection, Cancer Prevention and Genetic Engineering, Springer-Verlag, Berlin Heidelberg, 2003, pp. 1–126.

[3] A. Soares-Costa, L.M. Beltramini, O.H. Thiemann, F. Henrique-Silva, A sugarcane cystatin: recombinant expression purification & antifungal activity, Biochem. Biophys. Res. Commun. 296 (2002) 1194–1199.

[4] C.A. Ryan, The systemin signaling pathway: differential activation of plant defensive genes, Biochim. Biophys. Acta 1477 (2000) 112–121.

[5] D.C. Damasceno, G.T. Volpato, I.M. Calderon, R. Aguilar, M.V. Rudge, Effect of *Bauhinia forficata* extract in diabetic pregnant rats: maternal repercussions, Phytomedicine 11 (2004) 196–201.

[6] O.L. Zucchi, S. Moreira, E. F de Jesus, H.S. Neto, M.J. Salvador, Characterization of hypoglycemiant plants by total reflection X-ray fluorescence spectrometry, Biol. Trace Elem. Res. 103 (2005) 277–290.

[7] A. Pott, V.J. Pott, Plantas do Pantanal. Embrapa, Corumbá, 1994, pp. 320.

[8] C. Oliveira, L.A. Santana, A.K. Carmona, M.H. Cezari, M.U. Sampaio, C.A.M. Sampaio, M.L.V. Oliva, Structure of Cruzipain/Cruzain Inhibitors isolated from *Bauhinia bauhinioides* seeds, Biol. Chem. 382 (2001) 847–852.

[9] A.E. Eakin, A.A. Mills, G. Harth, J.H. McKerrow, C.S. Craik, The sequence, organization, and expression of the major cysteine protease (cruzipain) from *Trypanosoma cruzi*, J. Biol. Chem. 267 (1992) 7411–7420.

[10] C.J. Schofield, J. Jannin, R. Salvatella, The future of Chagas' disease control, Trends Parasitol. 22 (2006) 583–588.

[11] C. Neuhof, M.L. Oliva, D. Maybauer, M. Maybauer, C. Oliveira, M.U. Sampaio, C.A. Sampaio, H. Neuhof, Effect of plant Kunitz inhibitors from *Bauhinia bauhinioides* and *Bauhinia rufa* on pulmonary edema caused by activated neutrophils, Biol. Chem. 384 (2003) 939–944.

[12] M.L. Oliva, C.R. Mendes, M.A. Juliano, J.R. Chagas, J.C. Rosa, L.J. Greene, M.U. Sampaio, C.A.M. Sampaio, Characterization of a tissue kallikrein inhibitor isolated from *Bauhinia bauhinioides* seeds: inhibition of the hydrolysis of kininogen related substrates, Immunopharmacology 45 (1999) 163–169.

[13] M.V. Navarro, D.F. Vieira, R.A. Nagem, A.P. de Araújo, M.L. Oliva, R.C. Garratt, Crystallization and preliminary X-ray analysis of a novel Kunitz-type kallikrein inhibitor from *Bauhinia bauhinioides*, Acta Crystallogr. Sect. F Struct. Biol. Crystallogr. Commun. 61 (2005) 910–913.

[14] A.P.U. Araújo, D. Hansen, D.F. Vieira, C. Oliveira, L.A. Santana, L.M. Beltramini, C.A. M Sampaio, M.U. Sampaio, M.L.V. Oliva, Kunitz type *Bauhinia bauhinioides* inhibitors devoid of disulfide bridges: isolation of the cDNAs, heterologous expression and structural studies, Biol. Chem. 386 (2005) 561–568.

[15] M.C. Do Socorro, M.L.V. Oliva, H. Fritz, M. Jochum, R. Mentele, M.U. Sampaio, L.C.B.B. Coelho, I.F.C. Batista, C.A.M. Sampaio, Characterization of a Kunitz Trypsin Inhibitor with one disulfide bridge purified from *Swartzia pickellii*, Biochem. Biophys. Res. Commun. 291 (2002) 635–639.

[16] J.T. Sumikawa, A.M. Nakahata, H. Fritz, R. Mentele, M.U. Sampaio, M.L.V. Oliva, A Kunitz-type glycosylated elastase inhibitor with one disulfide bridge, Planta Med. 72 (2006) 393–397.

[17] A.M. Nakahata, N.R. Bueno, H.A. Rocha, C.R. Franco, R. Chammas, C.R. Nakaie, M.G. Jasiulionis, H.B. Nader, L.A. Santana, M.U. Sampaio, M.L. Oliva, Structural and inhibitory properties of a plant proteinase inhibitor containing the RGD motif, Int. J. Biol. Macromol. 40 (2006) 22–29.

[18] V. Turk, Review: targeting proteases: successes, failures and future prospects, Nat. Rev. 5 (2006) 785–799.

[19] C.A. Orengo, D.T. Jones, J.M. Thornton, Protein superfamilies and domain superfolds, Nature 372 (1994) 631–634.

[20] D. Mukhopadhyay, The molecular evolutionary history of a winged bean α-Chymotrypsin Inhibitor and modelling of its mutations through structural analises, J. Mol. Evol. 50 (2000) 214–223.

[21] A.G. Murzin, A.M. Lesk, C. Chothia, β-trefoil fold. Patterns of structure & sequence in the Kunitz Inhibitors, interleukins-1(and 1-(and fibroblast growth factors, J. Mol. Biol. 223 (1992) 531–543.

[22] R. Xu, Y. Xiau, A common sequence-associated physicochemical feature for proteins of beta-trefoil family, Comput. Biol. Chem. 29 (2005) 79–82.

[23] S. Onesti, P. Brick, D.M. Blow, Crystal structure of a Kunitz-type Tripsin Inhibitor from *Erythrina caffra* seeds, J. Mol. Biol. 217 (1991) 153–176.

[24] H.K. Song, S.W. Suh, Kunitz type Soybean Trypsin Inhibitor revisited: refined structure of its complex with porcine trypsin reveals an insight into the interaction between a homologous inhibitor from *Erythrina caffra* and tissue-type plasminogen activator, J. Mol. Biol. 275 (1998) 347–363.

[25] G.N. Ramachandran, V. Sasisekharan, Conformation of polypeptides and proteins, Adv. Protein Chem. 23 (1968) 383–438.

[26] B.J. Graves, M.H. Hatada, W.A. Hendrickson, J.K. Miller, V.S. Madison, Y. Satow, Structure of interleukin 1 at 2.7 angstrom resolution, Biochemistry 29 (1990) 2679–2684.

[27] H. Ago, Y. Kitagawa, A. Fujishima, Y. Matsura, Y. Katsube, Crystal structure of basic fibroblast growth factor at 1.6 Å resolution, J. Biochem. (Tokyo) 110 (1991) 360–363.

[28] J. Tetenbaum, L.M. Miller, A new spectroscopy approach to examining the role of disulfide bonds in the structure and unfolding of soybean trypsin inhibitor, Biochemistry 40 (2001) 12215–12219.

[29] K. Lehle, A. Wrba, R. Jaenicke, *Erythrina caffra* trypsin inhibitor retains its native structure and function after reducing its disulfide bonds, J. Mol. Biol. 239 (1994) 276–284.

[30] R. Sattar, S.A. Ali, M. Kamal, A.A. Khan, A. Abbasi, Molecular mechanism of enzyme inhibition: prediction of the three-dimensional structure of the dimeric trypsin inhibitor from *Leucaena leucocephala* by homology modelling, Biochem. Biophys. Res. Commun. 314 (2004) 755–765.

[31] S. Khamrui, J. Dasgupta, J.K. Dattagupta, U. Sem, Single mutation at P1 of a chymotrypsin inhibitor changes it to a trypsin inhibitor: X-Ray structural (2.15 Å) and biochemical basis, Biochimica et Biophysica Acta 1752 (2005) 65–72.

[32] M.A. Navia, B.M. McKeever, J.P. Springer, T.Y. Lin, H.R. Willians, E.M. Fluder, C.P. Dorn, K. Hoogsteen, Structure of human neutrophil elastase in complex with a peptide chloromethyl ketone inhibitor at 1.84 Å resolution, Biochemistry 86 (1989) 7–11.

[33] M. Tsunemi, Y. Matsuura, S. Sakakibara, Y. Katsube, Crystal structure of an Elastase-specific Inhibitor Elafin complexed with porcine pancreatic Elastase determined at 1.9 Å resolution, Biochemistry 35 (1996) 11570–11576.

[34] L.C. Alves, R.L. Melo, S.J. Sanderson, J.C. Mottram, G.H. Coombs, G. Caliendo, V. Santagada, L. Juliano, M.A. Juliano, S1 subsite specificity of a recombinant cysteine protease, CPB, of *Leishmania mexicana* compared with cruzain, human cathepsin L and papain using substrates containing non-natural basic amino acids, Eur. J. Biochem. 268 (2001) 1206–1212.

[35] A.G.W. Leslie, Joint CCP4 and ESF-EACMBNewsletters on Protein Crystallography, Vol. 26, Daresbury Laboratory, Warrington, UK, 1992.

[36] W. Kabsch, Evaluation of single-crystal X-ray diffraction data from a position-sensitive detector, J. Appl. Crystallogr. 21 (1988) 916–924.

[37] R.H. Blessing, An empirical correction for absorption anisotropy, Acta. Crystallogr. A51 (1995) 33–38.

[38] Collaborative Computational Project, Number 4, The CCP4 suite: programs for protein crystallography, Acta. Crystallogr. D50 (1994) 760–763.

[39] A. Vagin, A. Teplyakov, MOLREP: an automated program for molecular replacement, J. Appl. Crystallogr. 30 (1997) 1022–1025.

[40] T.A. Jones, J.Y. Zou, S.W. Cowan, M. Kjeldgaard, Improved methods for building protein models in electron density maps and the location of errors in these models, Acta Crystallogr. A47 (1991) 110–119.

[41] G.N. Murshudov, A. A Vagin, E.J. Dodson, Acta Crystallogr. D53 (1997) 240–255.

[42] R.A. Laskowski, M.W. MacArthur, D.S. Moss, J.M. Thornton, PROCHECK: a program to check the stereochemical quality of protein structures, J. Appl. Crystallogr. 26 (1993) 283–291.

[43] W.R. Pearson, Rapid and sensitive sequence comparison with FASTP and FASTA, Methods Enzymol. 183 (1990) 63–98.